LANGMUIR

pubs.acs.org/Langmuir Article

Construction of a Carbon Dots/Cobalt Oxyhydroxide Nanoflakes Biosensing Platform for Detection of Acid Phosphatase

Haijuan Zhang,[§] Yangxia Han,[§] Yali Yang, Jia Chen, and Hongdeng Qiu*

Cite This: https://doi.org/10.1021/acs.langmuir.1c01512 Read Online

ACCESS | Metrics & More | Article Recommendations | Supporting Information

ABSTRACT: Because abnormal acid phosphatase (ACP) can disrupt the normal physiological processes, determination of ACP level is extremely important for early diagnosis, treatment, and prognostic evaluation of diseases. Herein, a fluorescence platform for monitoring ACP level was established based on the assembly of red-emitting carbon dots (RCDs) on cobalt oxyhydroxide (CoOOH) nanoflakes. RCDs displayed excellent water solubility, pH stability, salt resistance, and photobleaching resistance. Interestingly, the fluorescence of the RCDs assembled on the surface of the CoOOH nanoflakes could be quenched due to the energy transfer caused by the nanoflakes. However, the ascorbic acid (AA) produced by the hydrolysis of ascorbic acid-2-phosphate trisodium salt (AAP) catalyzed by ACP could quickly and effectively reduce CoOOH nanoflakes, leading to the fluorescence recovery of the RCDs. Therefore, an "off−on" biosensor platform for rapid, sensitive, and selective detection of ACP was constructed with a limit of detection of 0.25 mU/L. With the assistance of the biosensor, the level of ACP in human serum samples was evaluated, and the spike recovery values ranged from 94.0% to 104.5%.

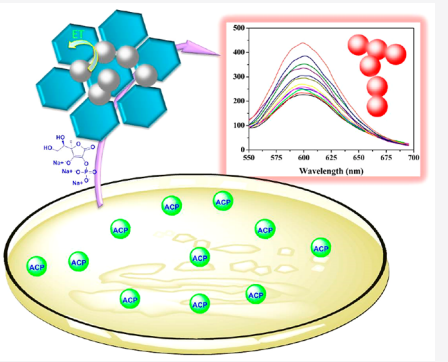

INTRODUCTION

Acid phosphatase (ACP), as a phosphomonoesterase widely distributed in many organisms and plant species, could hydrolyze effectively phosphate acid monoester to phosphate ion under weak acid conditions with its best catalytic performance.[1] Existing reports indicate that an abnormal ACP level is closely related to many important physiological processes. Generally, ACP levels are highly expressed in people who suffer from prostate cancer, Gaucher disease, granulocytic leukemia, Niemann Pick's disease, hemolytic anemia, osteosarcoma, osteitis deformans, and urinary retention. In particular, ACP not only can be used as a biomarker in the diagnosis of prostate cancer but also has significant value in the monitoring, curative effect observation, and prognosis evaluation of advanced prostate cancer. Therefore, the level of ACP is usually used as a serum marker to evaluate the above-mentioned diseases.[2−4] On the basis of the momentous role of ACP in physiology and clinical medicine, assay platforms including fluorescence, colorimetry, electrochemistry, SERS, mass spectrometric, and other methods for ACP sensing have been established.[5−13] Among them, fluorescence detection of ACP is considered one of the most widely used strategies due to its high sensitivity, convenient use, and simple operation.

As a typical 2D nanomaterial, cobalt oxyhydroxide (CoOOH) nanoflakes have attracted considerable research interest and are widely used in catalytic oxidation, photocarriers, supercapacitors, biological imaging, and biological sensing, etc., due to their excellent physical and chemical properties.[14−21] As an oxidant, CoOOH nanoflakes exhibit a planar structure and wide UV−vis absorption, making them an effective fluorescence quencher and energy acceptor for quenching the fluorescence of nanomaterials.[14] However, the fluorescence of the nanomaterial will be restored again when CoOOH nanoflakes are reduced by a reducing agent (such as ascorbic acid).[22] Therefore, CoOOH nanoflakes can be used as an intermediate for the detection of biological or other substances in fluorescence assay. Evolutionary, CoOOH nanoflakes have been widely used in recent years due to their excellent water dispersion and simple and mild preparation procedure. For example, based on the fluorescence quenching effect of the CoOOH nanoflakes, the determination of ascorbic acid oxidase, ochratoxin A, ascorbic acid, T4 polynucleotide kinase activity, vitamin C, imidacloprid, and ascorbic acid has been realized.[23−29]

Carbon dots (CDs) have aroused strong research interest because of their excellent water solubility, biocompatibility, photobleaching resistance, low toxicity, and easy modification.[30,31] In addition, due to the excellent physical and chemical properties of the CDs, they has become an emerging fluorescent nanomaterial which could replace traditional organic dyes, toxic semiconductor quantum dots, and weak

Received: June 6, 2021
Revised: August 10, 2021

https://doi.org/10.1021/acs.langmuir.1c01512
Langmuir XXXX, XXX, XXX−XXX

Scheme 1. Schematic Illustration of the Novel Fluorescence "Off−On" Nanosensor for ACP Assay Based on the Assembly of RCDs on CoOOH Nanoflakes

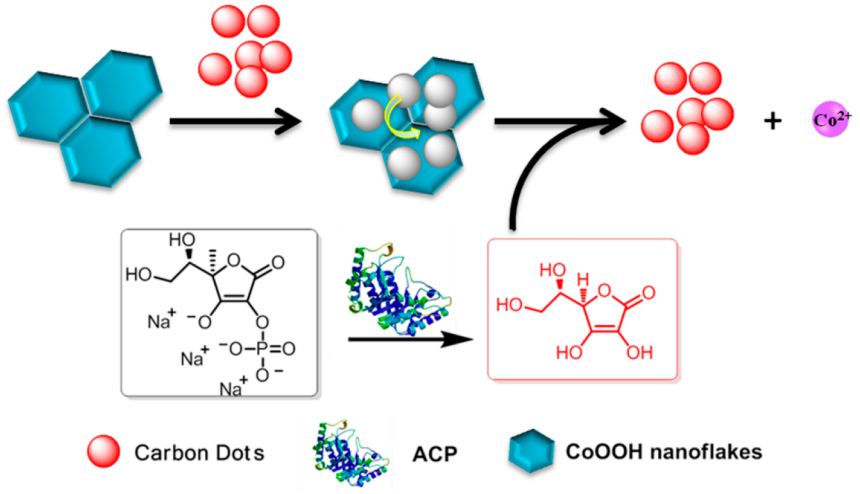

fluorescent polymers.[32−34] At present, CDs not only are widely used in drug delivery, optoelectronic devices, catalysis, energy, and other fields but also have attracted more attention in biosensor and biological imaging.[35,36] Unfortunately, due to the imperfection of the designability theory of long-wavelength fluorescent CDs, the emission wavelengths of most of the reported CDs are distributed in the blue and green regions. Therefore, the wide application of these CDs in biological imaging and biological samples detection is hindered because of the autofluorescence of amino acids, proteins, and other substances in biological samples or tissues.[37] Fortunately, the emergence of red-emitting carbon dots (RCDs) could compensate for the shortcomings of short-wavelength fluorescent nanomaterials.[38−41]

In this work, based on the excellent optical, chemical, and physical properties of the RCDs, a biosensor for selective detection of ACP level was established. RCDs with an emission wavelength of 607 nm were prepared using p-phenylenediamine (PPD) and PEG 1000 via a one-step solvothermal method, which could avoid the interference of autofluorescence of biological tissues and biological matrix. As shown in Scheme 1, RCDs were introduced into the CoOOH nanoflakes solution and integrated into the RCDs/CoOOH quenching system due to the energy transfer caused by CoOOH nanoflakes. The ascorbic acid (AA) produced by the ACP-catalyzed hydrolysis of ascorbic acid-2-phosphate trisodium salt (AAP) was used to decompose CoOOH nanoflakes into Co^{2+}, which caused the surface on which the RCDs were assembled to be decomposed and the fluorescence of the detection system was restored. Therefore, an "off−on" biosensor platform was constructed for rapid, sensitive, and selective detection of ACP. Importantly, the biosensor constructed based on the RCDs/CoOOH nanoflakes exhibited excellent performance in the assessment of ACP levels in human serum.

EXPERIMENTAL SECTION

Synthesis of the RCDs. RCDs were synthesized from PPD and PEG 1000 by a solvothermal method. Briefly, 1.0 mmol of PPD and 0.2 mmol of PEG 1000 (molar ratio 5:1) were dissolved in 60 mL of ethanol by sonication. The clear mixture was transferred into a Teflon-lined autoclave and heated to 160 °C for 2 h. When completed, the autoclave was cooled naturally to room temperature. The obtained deep purple/red mixture was filtered through a 0.45 μm filter membrane and stored at 4 °C for further use. In the control experiments, the molar ratios of PPD and PEG 1000 were changed to 10:1, 5:2, and 1:1. Other procedures were the same as above.

Synthesis of the CoOOH Nanoflakes. The CoOOH nanoflakes were synthesized by a previously reported chemical reaction method with some modification.[42] First, 0.8 M NaOH (1 mL) and 0.2 M NaClO (1 mL) were added dropwise into 1.0 mL of a 10 mM $CoCl_2$ solution under vigorous stirring. Then the mixture was sonicated for 30 min at room temperature to form a brownish black suspension. Subsequently, the mixture was rinsed three times with deionized water and dried at 80 °C. Finally, the as-synthesized CoOOH powder was redissolved with deionized water by sonication to form a 0.5 mg/mL homogeneous CoOOH nanoflakes solution and stored at 4 °C for further use.

Detection of ACP Activity in Buffer Solution. A 40 μL amount of freshly prepared CoOOH nanoflakes (5.0 mg/mL) and 20 μL of AAP (10 mM) were mixed in a series of 1.5 mL centrifuge tubes. Then 20 μL of ACP with various activities and a certain volume of phosphate buffer solution (20 mM PBS, pH 5.0) was added with a final volume of 0.99 mL and incubated at 37 °C for 15 min. Subsequently, 10 μL of RCDs was successively introduced, and the fluorescence spectra centered at 607 nm of the resulting solutions were measured on a Fluoromax-4 spectrofluorometer with an excitation of 540 nm.

Detection of ACP Activity in Human Serum. Three human serum samples pretreated and ultrafiltered to remove the redundant salt and small biomolecules were received from adult volunteers from the Second Affiliated Hospital of Lanzhou University, Lanzhou, PR China. Then the samples were diluted 10 times using PBS buffer (10 mM, pH = 5.0) and stored at 4 °C for further use. The feasibility of the assay was examined according to the above procedure by just adding the diluted human serum instead of the ACP standard solution.

RESULTS AND DISCUSSION

Optimization of Reaction Conditions for Synthesis of RCDs. The experimental conditions including reaction time, temperature, and ratio of reactants were optimized. The fluorescence intensity (FL intensity) of the prepared RCDs was increased when the reaction temperature changed from 140 to 160 °C and then decreased when the reaction temperature further increased to 200 °C (Figure S1A). Thus, the influence of reaction time on the FL intensity of the RCDs was studied at 160 °C (Figure S1B). The FL intensity of the RCDs increased until 2 h, remained almost constant with a

https://doi.org/10.1021/acs.langmuir.1c01512
Langmuir XXXX, XXX, XXX−XXX

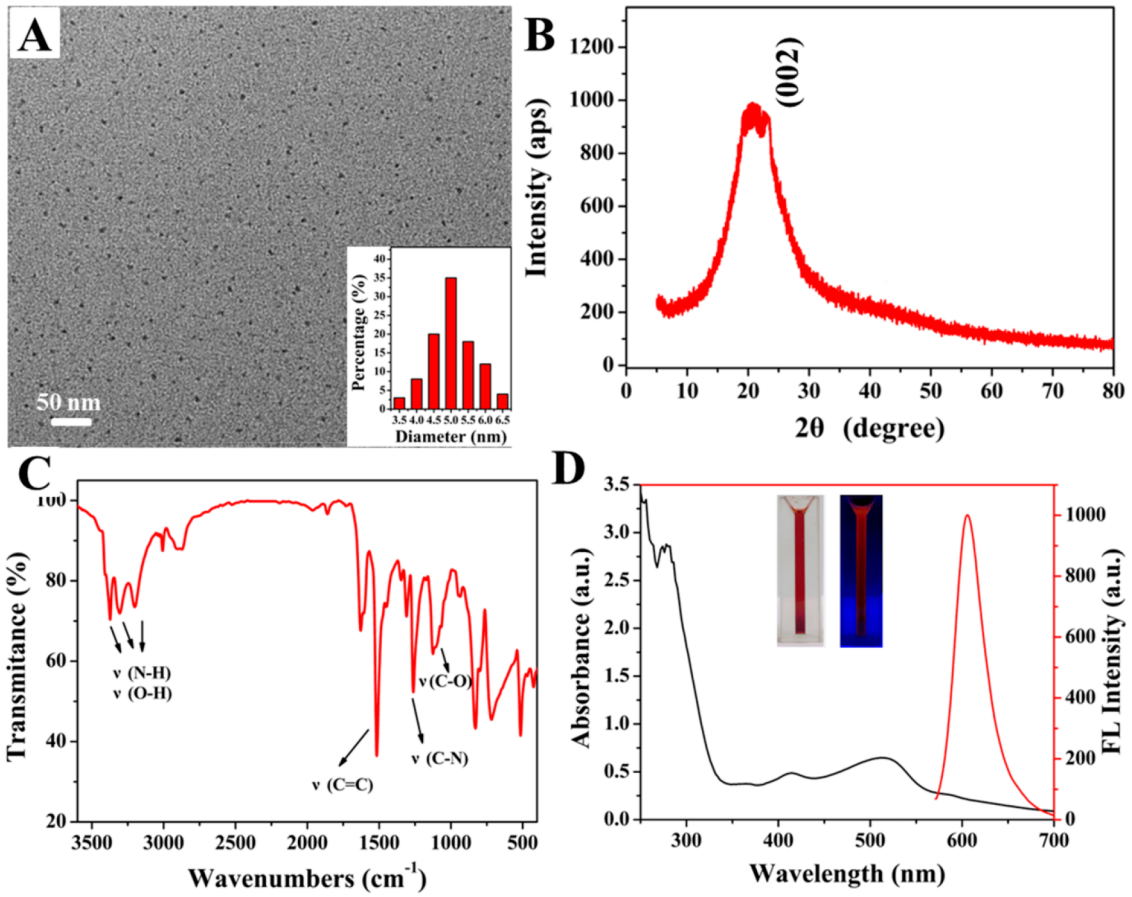

Figure 1. (A) TEM image, (B) XRD pattern, (C) FT-IR spectrum, and (D) UV−vis and fluorescent spectrum of the prepared RCDs.(Inset of A) Size distribution of the RCDs, which was calculated from 50 individual nanoparticles. (Inset of D) Pictures of the RCDs taken under visible light and UV light (λ_{ex} = 365 nm).

prolonged carbonization time of 2−4 h, and then decreased at 5 h. Therefore, in the subsequent experiments, the reaction temperature and time were set at 160 °C and 2 h, respectively. As the passivating agent played an important role in regulating the FL intensity of the prepared RCDs, the mass ratio between PPD and PEG 1000 was adjusted. As shown in Figure S1C, the FL intensity of the RCDs increased when the molar ratio was changed from 10:1 to 5:1 and decreased when the molar ratio changed from 5:1 to 1:1. Taking the fluorescent intensity into account, 5:1 was chosen as the optimal reagent ratio. The absolute quantum yield (QY) of the obtained RCDs was measured to be 25% under the excitation wavelength fixed at 540 nm.

Characterization of the RCDs and CoOOH Nanoflakes. The size and morphology of the prepared RCDs and CoOOH nanoflakes were characterized by TEM, XRD, and FT-IR. As illustrated in Figure 1A, the as-synthesized RCDs were uniform in size and well monodispersed, showing a spherical morphology with an average particle size of 5.0 nm. No obvious lattice fringes were found in the high-resolution TEM (HRTEM) of the RCDs (Figure S2A), indicating their amorphous nature. The XRD pattern of the RCDs displayed a prominent broad (002) diffraction peak centered at about 21° (Figure 1B), implying only graphitic carbon and no other crystalline phases,[43] which also confirmed the poor crystallization and the disordered surface of the RCDs. Raman spectroscopy was also used to identify the chemical state of carbon in the RCDs, as shown in Figure S2B. The D and G bands centered at 1402 and 1525 cm^{-1} are attributed to the disordered and sp^2-bonded C atoms in the RCDs, respectively. The relative intensity of the characteristic bands (I_D/I_G) was 0.91, which further confirmed the disordered graphite-like structure of the RCDs.[44] The FT-IR spectrum was also measured to identify the structures and functional groups of the RCDs, as shown in Figure 1C. The presence of N−H and O−H bonds was verified by the peaks centered at 3375, 3307, and 3200 cm^{-1}.[45] The adsorption peak at 1512 cm^{-1} was assigned to the vibration of C═C.[46] The peaks at 1254 and 1117 cm^{-1} proved the presence of C−N and C−O, respectively.[45] The above results proved that the RCDs were fabricated successfully.

The CoOOH nanoflakes were also fully characterized. TEM images (Figure 2A) clearly revealed the typical hexagon nanoflakes morphology of CoOOH, and a clear lattice could be observed in the HRTEM image (Figure 2B). The XRD pattern (Figure 2C) indicated the hexagonal rhomb-centered phase (JCPDS07-0169) of CoOOH nanoflakes, which proved the crystallinity of CoOOH nanoflakes.[47] The absorption peaks at 3386, 1628, and 578 cm^{-1} (Figure 2D) are ascribed to the hydroxyl group (−OH), Co−O bond, and Co−O^{2-} complex in the oxide, respectively.[18] Figure S3 shows that the prepared CoOOH nanoflakes had a completely different UV−vis spectral position from $CoCl_2$. In summary, the above results adequately demonstrated that the RCDs and CoOOH nanoflakes have been successfully fabricated. In addition, the morphology of the mixed system of RCDs and CoOOH

https://doi.org/10.1021/acs.langmuir.1c01512
Langmuir XXXX, XXX, XXX−XXX

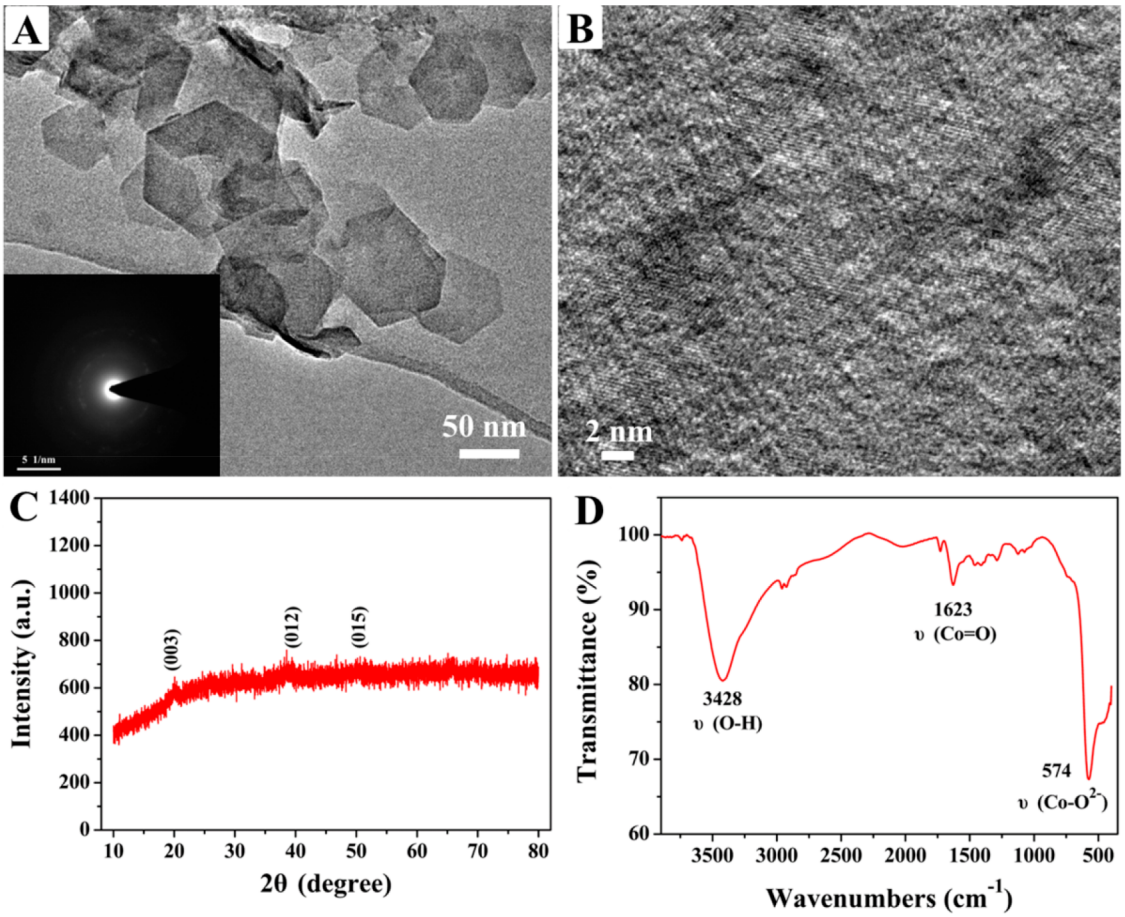

Figure 2. (A) TEM image, (B) HRTEM image, (C) XRD pattern, and (D) FT-IR spectrum of the CoOOH nanoflakes. (Inset of A) Selected-area electron diffraction (SAED) pattern of the CoOOH nanoflakes.

nanoflakes was also characterized. Figure S4 shows that the RCDs could be well assembled on CoOOH nanoflakes.

Optical Properties and Stability of the RCDs. The optical properties of the RCDs were investigated by UV−vis absorption and FL spectra, which are shown in Figure 1D. In the UV region, an absorption peak was observed at 255 nm with a shoulder at 280 nm, corresponding to the $\pi-\pi^*$ transitions of C═C and C═N bonds in the aromatic rings, respectively, which typically do not generate fluorescence.[48] The broad absorption peak around 513 nm could be adopted to excite the RCDs.[38] Unlike the generally reported CDs, the suspension of prepared RCDs showed an excitation-independent feature. When the excitation wavelength varied from 510 to 550 nm, no emission shift but increased FL intensities were obtained with the emission centered at 607 nm (Figure S5). This phenomenon could be ascribed to the relatively uniform size distribution and surface state of the prepared RCDs.[49] The FL intensities of the RCDs toward ionic strengths, pH, temperature, and light irradiation were measured to study the stability of the RCDs. As illustrated in Figure S6A and S6B, the RCDs exhibited stable FL intensity even in concentrations of NaCl up to 1.0 M or in the temperature range from 25 to 45 °C. Figure S6C demonstrates the FL intensity toward various pH values. The FL intensity increased with increasing pH from 3.0 to 7.0, followed by a decrease at higher pH values, which might result from changes in the surface charge due to protonation−deprotonation. Besides, the FL intensities were almost constant under continuous irradiation for 60 min (Figure S6D). The above phenomenon confirmed that the prepared RCDs possess excellent salt tolerance, excellent pH stability, and high photostability in an ambient environment, making them promising in biosensing and bioimaging. In addition, the influence of substances that may exist in biological tissues on the FL intensity of the RCDs has also been investigated. It can be seen from Figure S7A that these potential interfering substances could not affect the FL intensity of the RCDs. In addition, the AAP and ACP could not change the FL intensity of the RCDs (Figure S7B). These results are conducive to the application of RCDs in biological systems and biological samples.

Principle of the Biosensor. The design principle of the proposed biosensor for detecting ACP activity is described as follows. In detail, the fluorescence of the RCDs assembled on the surface of the CoOOH nanoflakes could be quenched effectively by the nanoflakes because it exhibited absorption peaks in a wide wavelength range (Figure S8) and overlapped with the fluorescence emission spectra of the RCDs. Therefore, the CoOOH nanoflakes have become a favorite fluorescence quenching agent and energy receptor.[50] However, the CoOOH nanoflakes are be reduced to Co^{2+} by adding AA, which was obtained by hydrolyzing AAP with ACP, causing the surface assembled by RCDs to be decomposed and the fluorescence to be restored. Figure 3A further verifies the rationality of the design of the biosensor and the feasibility of detecting ACP activity. Therefore, the RCDs could realize effectively the "off−

https://doi.org/10.1021/acs.langmuir.1c01512
Langmuir XXXX, XXX, XXX−XXX

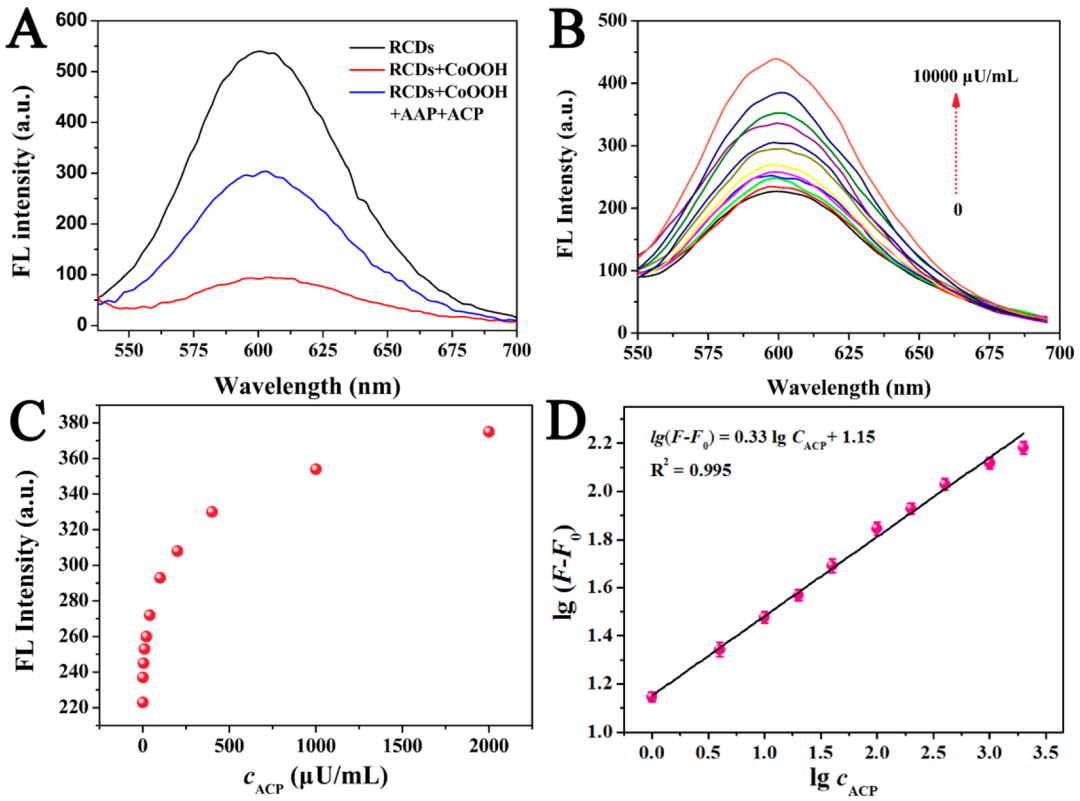

Figure 3. (A) Fluorescence quenching and recovery of the RCDs by CoOOH and ACP (concentrations of CoOOH, AAP, and ACP were 200 μg/mL, 200 μM, and 16 μU/mL, respectively). (B–D) Fluorescence emission spectra and FL intensities of the RCDs–CoOOH with varied concentrations of ACP.

Table 1. Comparison of Our Approach with Other Methods for ACP Detection

detection strategy	material	intermedium	linear range	LOD	total detection time	ref
fluorescence	N-GQDs	AA2P, dopaquinone	0.04–0.7 U/L	14 mU/L	40 min	51
	GQDs@GSH	AA2P	0.1–9 U/L	27 mU/L	40 min	52
	N-CDs	AA2P	5–40 U/L	0.1 U/L	~120 min	6
	L-cys-$CuInS_2$ QDs	$(NaPO_3)_6$	75–1500 μU/L	9.02 μU/L	2 min	53
	Au-NCs/MnO_2	AA2P	0.01–16 U/L	3 mU/L	60 min	54
	GQDs	$Cr_2O_7^{2-}$, AA2P	0.02–3 U/L	8.9 mU/L	~120 min	55
	CQD	PPi, Ni^{2+}	18.2–1300 U/L	5.5 U/L	60 min	56
	CDs	dopamine	1–60 U/L	0.45 U/L	100 min	57
	GQDs-NR	lecithin/β-CD complex	0–1500 mU/L	28 mU/L	90 min	58
	N-CDs	$(NaPO_3)_6$	1–50 U/L	0.43 U/L	120 min	59
colorimetric	$Cu(BCDS)_2^{2-}$	AA2P	0–220 U/L	3.16 U/L	30 min	60
	Ch–PtNPs	AA2P, TMB	0.25–2.5 U/L	16 mU/L	35 min	7
	C_3N_4	Cu^{2+}–PPi, TMB	0.05–40 U/L	8.8 mU/L	45 min	8
electrochemical	TNA/g-C_3N_4/DAT	Fe^{3+}, AA2P	0.05–100 U/L	16 mU/L	15 min	61
	RCDs/CoOOH	AAP	1–2000 mU/L	0.25 mU/L	15 min	this work

on" mode detection of ACP based on the CoOOH nanoflakes and AAP intermediates.

Sensitivity and Selectivity of the Biosensor. To achieve sensitive and rapid detection of ACP activity, some factors that affect the fluorescence intensity of the detection system, including the concentration of the CoOOH nanoflakes and AA, pH value of the buffer solution, fluorescence quenching, and recovery time were investigated. As expected, the fluorescence intensity of the RCDs solution gradually decreased with increasing CoOOH nanoflakes concentration. The fluorescence intensity was less than 100 a.u. when the concentration of the CoOOH nanoflakes decreased to 200 μg/mL (Figure S9). Therefore, the concentration of CoOOH nanoflakes was selected as 200 μg/mL in the subsequent experiments. Similarly, the change of fluorescence intensity of the RCDs/CoOOH system was opposite to that of the above detection system, that is, the concentration of AA was positively correlated with the fluorescence intensity of the RCDs (Figure S10). Therefore, the concentration of AA and AAP was designated as 200 μM in the subsequent experiments. In addition, Figure S11 shows that the fluorescence intensity of the RCDs returned to the maximum when the pH of the buffer solution was 5.0. Subsequently, the fluorescence quenching and recovery times of the RCDs by CoOOH nanoflakes and ACP+AAP were determined. Figure S12 shows that the CoOOH nanoflakes could quench the fluorescence of the

https://doi.org/10.1021/acs.langmuir.1c01512
Langmuir XXXX, XXX, XXX–XXX

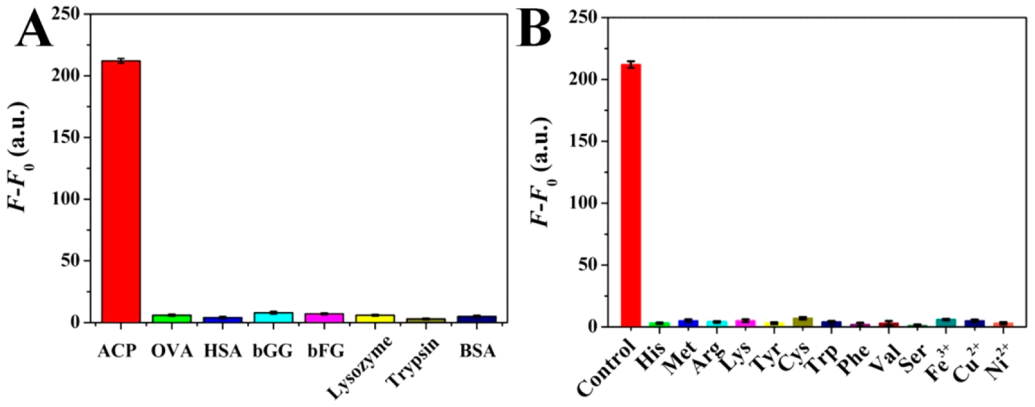

Figure 4. Fluorescence responses of the system toward ACP (2000 μU/mL) and other interfering agents (50 μmol/L) (ovalbumin, OVA; human serum albumin, HSA; bovine albumin, BSA; bovine gamma globulin solution, bGG; fibrinogen, bFG).

RCDs in a very short time (1 min). The response time of the RCDs/CoOOH system to ACP+AAP reached equilibrium within 15 min. Therefore, 1 and 15 min were used as effective fluorescence quenching and recovery times, respectively.

Subsequently, the proposed biosensor was applied for evaluation of the ACP level. It can be seen from Figure 3B that the gradually increasing concentration of ACP causes the fluorescence of the detection system to gradually increase, and this phenomenon is shown in Figure 3C. In addition, a good linear relationship was obtained when the concentration of ACP ranged from 1 to 2000 mU/L with a limit of detection of 0.25 mU/L (Figure 3D). The sensitivity, detection time, and other properties for ACP sensing based on the proposed biosensor were comparable to or even lower than reported (Table 1). Furthermore, some potential interfering substances (protein, amino acid, and cation, etc) and metal ions in the organism hardly change the fluorescence intensity of the detection system (Figure 4), which proved that these substances could not affect the detection performance of the proposed biosensor for ACP. The above results demonstrated that the biosensor can evaluate ACP levels quickly, sensitively, and selectively based on the RCDs/CoOOH system.

Determination of ACP by Biosensor in Real Samples. To verify the feasibility of the fluorescence method based on the RCDs to detect ACP in actual samples and expand its application range, the ACP levels in three human serum samples were evaluated. Table 2 shows that there were obvious differences in ACP level for different samples. Subsequently, ACP levels in human serum samples were determined by the standard addition method, and satisfactory spiked recoveries (94.0−104.5%) were obtained. The above results proved that the method could realize the assessment of ACP level and has potential value in practical application, which is expected to provide a useful platform for the diagnosis, treatment, and prognosis evaluation of ACP-related diseases.

Table 2. Determination of ACP in Human Serum Samples

human serum	detected (mU/mL)	added (mU/mL)	found (mU/mL)	recovery (%)	RSD (%)
1	58.4	5.0	63.2	96.0	5.8
		10.0	67.9	95.0	4.6
		20.0	79.3	104.5	3.9
2	47.8	5.0	52.5	94.0	2.8
		10.0	58.1	103.0	1.9
		20.0	67.4	98.0	3.2
3	62.7	5.0	67.8	102.0	4.8
		10.0	73.1	104.0	2.7
		20.0	82.4	98.5	3.6

CONCLUSION

RCDs with excellent resistance to pH, NaCl, temperature, and long-lasting light radiation were fabricated by a one-pot solvothermal method. The fluorescence of the obtained RCDs could be quenched effectively by the CoOOH nanoflakes because the assembly of the RCDs on the surface of the CoOOH nanoflakes shortened the distance between them, which further promoted the energy transfer of the RCDs to the CoOOH nanoflakes. Interestingly, AA could reduce CoOOH nanoflakes to Co^{2+}. Therefore, a fluorescence method based on the RCDs biosensor for rapid, sensitive, and selective detection of ACP activity was established with a limit of detection of 0.25 mU/L. In addition, the RCDs could assess successfully the ACP level in human serum samples, indicating that they displayed excellent practical application capabilities and were expected to provide useful reference for the diagnosis, treatment, and prognosis evaluation of diseases related to ACP level.

ASSOCIATED CONTENT

Supporting Information

The Supporting Information is available free of charge at https://pubs.acs.org/doi/10.1021/acs.langmuir.1c01512.

Details about the reagents and apparatuses; additional figures (PDF)

AUTHOR INFORMATION

Corresponding Author

Hongdeng Qiu − *CAS Key Laboratory of Chemistry of Northwestern Plant Resources and Key Laboratory for Natural Medicine of Gansu Province, Lanzhou Institute of Chemical Physics, Chinese Academy of Sciences, Lanzhou 730000, China; College of Chemistry, Zhengzhou University, Zhengzhou 450001, China; School of Chemistry and Chemical Engineering, Gannan Normal University, Ganzhou 341000, China;* orcid.org/0000-0002-2702-9415; Email: hdqiu@licp.cas.cn

https://doi.org/10.1021/acs.langmuir.1c01512
Langmuir XXXX, XXX, XXX−XXX

Authors

Haijuan Zhang − *CAS Key Laboratory of Chemistry of Northwestern Plant Resources and Key Laboratory for Natural Medicine of Gansu Province, Lanzhou Institute of Chemical Physics, Chinese Academy of Sciences, Lanzhou 730000, China; State Key Laboratory of Grassland Agro-Ecosystem, Institute of Innovation Ecology, Lanzhou University, Lanzhou 730000, China*

Yangxia Han − *CAS Key Laboratory of Chemistry of Northwestern Plant Resources and Key Laboratory for Natural Medicine of Gansu Province, Lanzhou Institute of Chemical Physics, Chinese Academy of Sciences, Lanzhou 730000, China*

Yali Yang − *CAS Key Laboratory of Chemistry of Northwestern Plant Resources and Key Laboratory for Natural Medicine of Gansu Province, Lanzhou Institute of Chemical Physics, Chinese Academy of Sciences, Lanzhou 730000, China*

Jia Chen − *CAS Key Laboratory of Chemistry of Northwestern Plant Resources and Key Laboratory for Natural Medicine of Gansu Province, Lanzhou Institute of Chemical Physics, Chinese Academy of Sciences, Lanzhou 730000, China*

Complete contact information is available at: https://pubs.acs.org/10.1021/acs.langmuir.1c01512

Author Contributions

[§]H.Z. and Y.H. contributed equally to this work.

Author Contributions

H.Z. and Y.H. conducted most of the experiments and data analyses and wrote the manuscript. Y.Y. performed some experiments related to the fluorescent nanomaterials. J.C. made some suggestions for the manuscript. H.Q. finalized the paper. The manuscript was discussed through contributions of all authors. All authors have given approval to the final version of the manuscript.

Notes

The authors declare no competing financial interest.

■ ACKNOWLEDGMENTS

The authors are grateful for financial support from the National Natural Science Foundation of China (Nos. 22074154 and 21822407), Gansu Youth Science and Technology Fund Project (20JR10RA051), and Gansu Innovation Group Project (20JR5RA573).

■ REFERENCES

(1) Bull, H.; Murray, P. G.; Thomas, D.; Fraser, A. M.; Nelson, P. N. Acid Phosphatases. *Mol. Pathol.* **2002**, *55* (2), 65−72.

(2) Leman, E. S.; Getzenberg, R. H. Biomarkers for Prostate Cancer. *J. Cell. Biochem.* **2009**, *108* (1), 3−9.

(3) Schiffer, E. Biomarkers for Prostate Cancer. *World J. Urol.* **2007**, *25* (6), 557−562.

(4) Makarov, D. V.; Loeb, S.; Getzenberg, R. H.; Partin, A. W. Biomarkers for Prostate Cancer. *Annu. Rev. Med.* **2009**, *60* (1), 139−151.

(5) Wang, H.; Wang, X.; Kong, R.-M.; Xia, L.; Qu, F. Metal-Organic Framework as a Multi-Component Sensor for Detection of Fe^{3+}, Ascorbic Acid and Acid Phosphatase. *Chin. Chem. Lett.* **2021**, *32* (1), 198−202.

(6) Zhu, Z.; Lin, X.; Wu, L.; Zhao, C.; Zheng, Y.; Liu, A.; Lin, L.; Lin, X. Switch-on" Fluorescent Nanosensor Based on Nitrogen-Doped Carbon Dots-MnO_2 Nanocomposites for Probing the Activity of Acid Phosphatase. *Sens. Actuators, B* **2018**, *274*, 609−615.

(7) Deng, H.-H.; Lin, X.-L.; Liu, Y.-H.; Li, K.-L.; Zhuang, Q.-Q.; Peng, H.-P.; Liu, A.-L.; Xia, X.-H.; Chen, W. Chitosan-Stabilized Platinum Nanoparticles as Effective Oxidase Mimics for Colorimetric Detection of Acid Phosphatase. *Nanoscale* **2017**, *9* (29), 10292−10300.

(8) Guo, Y.; Li, X.; Dong, Y.; Wang, G.-L. Acid Phosphatase Invoked Exquisite Enzyme Cascade for Amplified Colorimetric Bioassay. *ACS Sustainable Chem. Eng.* **2019**, *7* (8), 7572−7579.

(9) Bi, Q.; Qiu, F.; Yuan, R.; Xiang, Y. In Situ Formation of G-Quadruplex/Hemin Nanowires for Sensitive and Label-Free Electrochemical Sensing of Acid Phosphatase. *Sens. Actuators, B* **2021**, *330*, 129272.

(10) Gan, X.; Qiu, F.; Jiang, B.; Yuan, R.; Xiang, Y. Convenient and Highly Sensitive Electrochemical Biosensor for Monitoring Acid Phosphatase Activity. *Sens. Actuators, B* **2021**, *332*, 129483.

(11) Li, X.; Li, B.; Hong, J.; Zhou, X. Highly Selective Determination of Acid Phosphatase in Biological Samples Using a Biomimetic Recognition-Based Sers Sensor. *Sens. Actuators, B* **2018**, *276*, 421−428.

(12) Han, Y.; Quan, K.; Chen, J.; Qiu, H. Advances and Prospects on Acid Phosphatase Biosensor. *Biosens. Bioelectron.* **2020**, *170*, 112671.

(13) Ma, Q. L.; Chen, Y. L.; Feng, N.; Yan, F.; Ju, H. X. A MALDI-MS Sensing Chip Prepared by Non-Covalent Assembly for Quantitation of Acid Phosphatase. *Sci. China: Chem.* **2021**, *64* (1), 151−156.

(14) Mei, T.; Zhang, S.; Sun, J.; Hu, Y. 2D CoOOH Nanosheets as Oxidase Mimic for the Colorimetric Assay of Sulfite in Food. *Anal. Methods* **2021**, *13* (6), 764−768.

(15) Chen, H.; Wang, H.; Xia, W.; Zhang, J.; Wang, L. Upconversion Luminescence Detection of Ascorbic Acid Based on $NaGdF_4$:Yb,Er@$NaYF_4$ Nanoparticles and Oxidase-Like CoOOH Nanoflakes. *Anal. Methods* **2020**, *12* (42), 5081−5085.

(16) Zhou, J.; Ling, Y.; Li, N. B.; Luo, H. Q. Fluorometric and Resonance Rayleigh Scattering Dual-Mode Bioprobe for Determination Of the Activity of Alkaline Phosphatase based on the Use Of CoOOH Nanoflakes and Cobalt(II)-Dependent Dnazyme-Assisted Amplification. *Microchim. Acta* **2019**, *186* (7), 437.

(17) Liu, S. G.; Han, L.; Li, N.; Xiao, N.; Ju, Y. J.; Li, N. B.; Luo, H. Q. A Fluorescence and Colorimetric Dual-Mode Assay of Alkaline Phosphatase Activity Via Destroying Oxidase-Like Coooh Nanoflakes. *J. Mater. Chem. B* **2018**, *6* (18), 2843−2850.

(18) Huang, J.; Shang, Q.; Huang, Y.; Tang, F.; Zhang, Q.; Liu, Q.; Jiang, S.; Hu, F.; Liu, W.; Luo, Y.; Yao, T.; Jiang, Y.; Pan, Z.; Sun, Z.; Wei, S. Oxyhydroxide Nanosheets with Highly Efficient Electron-Hole Pair Separation for Hydrogen Evolution. *Angew. Chem., Int. Ed.* **2016**, *55* (6), 2137−2141.

(19) Huang, J. H.; Chen, J. T.; Yao, T.; He, J. F.; Jiang, S.; Sun, Z. H.; Liu, Q. H.; Cheng, W. R.; Hu, F. C.; Jiang, Y.; Pan, Z. Y.; Wei, S. Q. CoOOH Nanosheets with High Mass Activity for Water Oxidation. *Angew. Chem., Int. Ed.* **2015**, *54* (30), 8722−8727.

(20) Feng, L.-L.; Wu, Y.-X.; Zhang, D.-L.; Hu, X.-X.; Zhang, J.; Wang, P.; Song, Z.-L.; Zhang, X.-B.; Tan, W. Near Infrared Graphene Quantum Dots-Based Two-Photon Nanoprobe for Direct Bioimaging of Endogenous Ascorbic Acid in Living Cells. *Anal. Chem.* **2017**, *89* (7), 4077−4084.

(21) Zhang, L.; Dutta, A. K.; Jarero, G.; Stroeve, P. Nucleation and Growth of Cobalt Hydroxide Crystallites in Organized Polymeric Multilayers. *Langmuir* **2000**, *16* (17), 7095−7100.

(22) Wu, Z. H.; Nan, D. Y.; Yang, H.; Pan, S.; Liu, H.; Hu, X. L. A Ratiometric Fluorescence-Scattered Light Strategy Based on MoS_2 Quantum Dots/CoOOH Nanoflakes System for Ascorbic Acid Detection. *Anal. Chim. Acta* **2019**, *1091*, 59−68.

(23) Li, N.; Zhang, F.; Sun, W.; Zhang, L.; Su, X. Redox Reaction-Modulated Fluorescence Biosensor for Ascorbic Acid Oxidase Assay by Using MoS_2 Quantum Dots as Fluorescence Probe. *Talanta* **2021**, *222*, 121522.

(24) Bi, X.; Luo, L.; Li, L.; Liu, X.; Chen, B.; You, T. A Fret-Based Aptasensor for Ochratoxin a Detection Using Graphitic Carbon

Nitride Quantum Dots and CoOOH Nanosheets as Donor-Acceptor Pair. *Talanta* **2020**, *218*, 121159.
(25) Li, L.; Wang, C.; Liu, K.; Wang, Y.; Liu, K.; Lin, Y. Hexagonal Cobalt Oxyhydroxide-Carbon Dots Hybridized Surface: High Sensitive Fluorescence Turn-on Probe for Monitoring of Ascorbic Acid in Rat Brain Following Brain Ischemia. *Anal. Chem.* **2015**, *87* (6), 3404−3411.
(26) Meng, H.-M.; Zhang, X.-B.; Yang, C.; Kuai, H.; Mao, G.-J.; Gong, L.; Zhang, W.; Feng, S.; Chang, J. Efficient Two-Photon Fluorescence Nanoprobe for Turn-on Detection and Imaging of Ascorbic Acid in Living Cells and Tissues. *Anal. Chem.* **2016**, *88* (11), 6057−6063.
(27) Cen, Y.; Yang, Y.; Yu, R.-Q.; Chen, T.-T.; Chu, X. A Cobalt Oxyhydroxide Nanoflake-Based Nanoprobe for the Sensitive Fluorescence Detection of T4 Polynucleotide Kinase Activity and Inhibition. *Nanoscale* **2016**, *8* (15), 8202−8209.
(28) Lu, Q.; Chen, X.; Liu, D.; Wu, C.; Liu, M.; Li, H.; Zhang, Y.; Yao, S. A Turn-on Fluorescent Probe for Vitamin C Based on the Use of a Silicon/CoOOH Nanoparticle System. *Microchim. Acta* **2019**, *186* (2), 72.
(29) Li, H.; Jin, R.; Kong, D.; Zhao, X.; Liu, F.; Yan, X.; Lin, Y.; Lu, G. Switchable Fluorescence Immunoassay Using Gold Nanoclusters Anchored Cobalt Oxyhydroxide Composite for Sensitive Detection of Imidacloprid. *Sens. Actuators, B* **2019**, *283*, 207−214.
(30) Li, C.; Zhang, J.; Jiang, H.; Wang, X.; Liu, J. Orthogonal Adsorption of Carbon Dots and DNA on Nanoceria. *Langmuir* **2020**, *36* (9), 2474−2481.
(31) Kumari, R.; Sahu, S. K. Effect of Solvent-Derived Highly Luminescent Multicolor Carbon Dots for White-Light-Emitting Diodes and Water Detection. *Langmuir* **2020**, *36* (19), 5287−5295.
(32) Sun, Y.-P.; Zhou, B.; Lin, Y.; Wang, W.; Fernando, K. A. S.; Pathak, P.; Meziani, M. J.; Harruff, B. A.; Wang, X.; Wang, H.; Luo, P. G.; Yang, H.; Kose, M. E.; Chen, B.; Veca, L. M.; Xie, S.-Y. Quantum-Sized Carbon Dots for Bright and Colorful Photoluminescence. *J. Am. Chem. Soc.* **2006**, *128* (24), 7756−7757.
(33) Tong, L.; Wang, X.; Chen, Z.; Liang, Y.; Yang, Y.; Gao, W.; Liu, Z.; Tang, B. One-Step Fabrication of Functional Carbon Dots with 90% Fluorescence Quantum Yield for Long-Term Lysosome Imaging. *Anal. Chem.* **2020**, *92* (9), 6430−6436.
(34) Zhou, Y.; Mintz, K. J.; Sharma, S. K.; Leblanc, R. M. Carbon Dots: Diverse Preparation, Application, and Perspective in Surface Chemistry. *Langmuir* **2019**, *35* (28), 9115−9132.
(35) Miao, X.; Yan, X.; Qu, D.; Li, D.; Tao, F. F.; Sun, Z. Red Emissive Sulfur, Nitrogen Codoped Carbon Dots and Their Application in Ion Detection and Theraonostics. *ACS Appl. Mater. Interfaces* **2017**, *9* (22), 18549−18556.
(36) Su, D.; Han, X.; Yan, X.; Jin, R.; Li, H.; Kong, D.; Gao, H.; Liu, F.; Sun, P.; Lu, G. Smartphone-Assisted Robust Sensing Platform for on-Site Quantitation of 2,4-Dichlorophenoxyacetic Acid Using Red Emissive Carbon Dots. *Anal. Chem.* **2020**, *92* (18), 12716−12724.
(37) Sun, S.; Zhang, L.; Jiang, K.; Wu, A.; Lin, H. Toward High-Efficient Red Emissive Carbon Dots: Facile Preparation, Unique Properties, and Applications as Multifunctional Theranostic Agents. *Chem. Mater.* **2016**, *28* (23), 8659−8668.
(38) Liu, Y.; Duan, W.; Song, W.; Liu, J.; Ren, C.; Wu, J.; Liu, D.; Chen, H. Red Emission B, N, S-Co-Doped Carbon Dots for Colorimetric and Fluorescent Dual Mode Detection of Fe^{3+} Ions in Complex Biological Fluids and Living Cells. *ACS Appl. Mater. Interfaces* **2017**, *9* (14), 12663−12672.
(39) Ali, H.; Bhunia, S. K.; Dalal, C.; Jana, N. R. Red Fluorescent Carbon Nanoparticle-Based Cell Imaging Probe. *ACS Appl. Mater. Interfaces* **2016**, *8* (14), 9305−9313.
(40) Li, H.; Su, D.; Gao, H.; Yan, X.; Kong, D.; Jin, R.; Liu, X.; Wang, C.; Lu, G. Design of Red Emissive Carbon Dots: Robust Performance for Analytical Applications in Pesticide Monitoring. *Anal. Chem.* **2020**, *92* (4), 3198−3205.
(41) Ding, H.; Wei, J.-S.; Zhong, N.; Gao, Q.-Y.; Xiong, H.-M. Highly Efficient Red-Emitting Carbon Dots with Gram-Scale Yield for Bioimaging. *Langmuir* **2017**, *33* (44), 12635−12642.
(42) Zheng, M.; Xie, Z.; Qu, D.; Li, D.; Du, P.; Jing, X.; Sun, Z. On-Off-on Fluorescent Carbon Dot Nanosensor for Recognition of Chromium(VI) and Ascorbic Acid Based on the Inner Filter Effect. *ACS Appl. Mater. Interfaces* **2013**, *5* (24), 13242−13247.
(43) Teng, X.; Ma, C.; Ge, C.; Yan, M.; Yang, J.; Zhang, Y.; Morais, P. C.; Bi, H. Green Synthesis of Nitrogen-Doped Carbon Dots from Konjac Flour with "Off-on" Fluorescence by Fe^{3+} and L-Lysine for Bioimaging. *J. Mater. Chem. B* **2014**, *2* (29), 4631−4639.
(44) Hu, Y.; Yang, J.; Tian, J.; Jia, L.; Yu, J.-S. Waste Frying Oil as a Precursor for One-Step Synthesis of Sulfur-Doped Carbon Dots with pH-Sensitive Photoluminescence. *Carbon* **2014**, *77*, 775−782.
(45) Zhang, H.; Zhang, B.; Di, C.; Ali, M. C.; Chen, J.; Li, Z.; Si, J.; Zhang, H.; Qiu, H. Label-Free Fluorescence Imaging of Cytochrome C in Living Systems and Anti-Cancer Drug Screening with Nitrogen Doped Carbon Quantum Dots. *Nanoscale* **2018**, *10* (11), 5342−5349.
(46) Zhang, H.; Chen, J.; Yang, Y.; Wang, L.; Li, Z.; Qiu, H. Discriminative Detection of Glutathione in Cell Lysates Based on Oxidase-Like Activity of Magnetic Nanoporous Graphene. *Anal. Chem.* **2019**, *91* (8), 5004−5010.
(47) Liu, J.; Tang, D.; Chen, Z.; Yan, X.; Zhong, Z.; Kang, L.; Yao, J. Chemical Redox Modulated Fluorescence of Nitrogen-Doped Graphene Quantum Dots for Probing the Activity of Alkaline Phosphatase. *Biosens. Bioelectron.* **2017**, *94*, 271−277.
(48) Ding, H.; Yu, S.-B.; Wei, J.-S.; Xiong, H.-M. Full-Color Light-Emitting Carbon Dots with a Surface-State-Controlled Luminescence Mechanism. *ACS Nano* **2016**, *10* (1), 484−491.
(49) Peng, H.; Li, Y.; Jiang, C.; Luo, C.; Qi, R.; Huang, R.; Duan, C.-G.; Travas-Sejdic, J. Tuning the Properties of Luminescent Nitrogen-Doped Carbon Dots by Reaction Precursors. *Carbon* **2016**, *100*, 386−394.
(50) Han, Y.; Chen, J.; Li, Z.; Chen, H.; Qiu, H. Recent Progress and Prospects of Alkaline Phosphatase Biosensor Based on Fluorescence Strategy. *Biosens. Bioelectron.* **2020**, *148*, 111811.
(51) Qu, Z.; Na, W.; Liu, X.; Liu, H.; Su, X. A Novel Fluorescence Biosensor for Sensitivity Detection of Tyrosinase and Acid Phosphatase Based on Nitrogen-Doped Graphene Quantum Dots. *Anal. Chim. Acta* **2018**, *997*, 52−59.
(52) Qu, Z.; Li, N.; Na, W.; Su, X. A Novel Fluorescence "Turn Off-on" Nanosensor for Sensitivity Detection Acid Phosphatase and Inhibitor Based on Glutathione-Functionalized Graphene Quantum Dots. *Talanta* **2019**, *192*, 61−68.
(53) Liu, Z.; Lin, Z.; Liu, L.; Su, X. A Convenient and Label-Free Fluorescence "Turn Off-on" Nanosensor with High Sensitivity and Selectivity for Acid Phosphatase. *Anal. Chim. Acta* **2015**, *876*, 83−90.
(54) Xu, M.; Ma, R.; Huang, C.; Shi, G.; Zhou, T.; Deng, J. Competitive Redox Reaction of Au-NCs/MnO_2 Nanocomposite: Toward Colorimetric and Fluorometric Detection of Acid Phosphatase as an Indicator of Soil Cadmium Contamination. *Anal. Chim. Acta* **2020**, *1096*, 174−183.
(55) Shi, F.; Zhang, Y.; Na, W.; Zhang, X.; Li, Y.; Su, X. Graphene Quantum Dots as Selective Fluorescence Sensor for the Detection of Ascorbic Acid and Acid Phosphatase Via Cr (VI)/Cr (III)-Modulated Redox Reaction. *J. Mater. Chem. B* **2016**, *4* (19), 3278−3285.
(56) Qian, Z.; Chai, L.; Zhou, Q.; Huang, Y.; Tang, C.; Chen, J.; Feng, H. Reversible Fluorescent Nanoswitch Based on Carbon Quantum Dots Nanoassembly for Real-Time Acid Phosphatase Activity Monitoring. *Anal. Chem.* **2015**, *87* (14), 7332−7339.
(57) Chen, Y.; Wang, Z.; Hao, X.; Li, F.; Zheng, Y.; Zhang, J.; Lin, X.; Weng, S. Selective and Sensitive Fluorescent Monitoring of Acid Phosphatase (ACP) Activity under Neutral Conditions through the ACP Enzymatic Catalysis of Dopamine as a New Substrate to Polydopamine. *Sens. Actuators, B* **2019**, *297*, 126784.
(58) Na, W.; Liu, Q.; Sui, B.; Hu, T.; Su, X. Highly Sensitive Detection of Acid Phosphatase by Using a Graphene Quantum Dots-Based Förster Resonance Energy Transfer. *Talanta* **2016**, *161*, 469−475.
(59) Zhu, Z.; Lin, X.; Wu, L.; Zhao, C.; Li, S.; Liu, A.; Lin, X.; Lin, L. Nitrogen-Doped Carbon Dots as a Ratiometric Fluorescent Probe for Determination of the Activity of Acid Phosphatase, for Inhibitor

https://doi.org/10.1021/acs.langmuir.1c01512
Langmuir XXXX, XXX, XXX−XXX

Screening, and for Intracellular Imaging. *Microchim. Acta* **2019**, *186* (8), 558.
(60) Hu, Q.; Zhou, B.; Li, F.; Kong, J.; Zhang, X. Turn-on Colorimetric Platform for Dual Activity Detection of Acid and Alkaline Phosphatase in Human Whole Blood. *Chem. - Asian J.* **2016**, *11* (21), 3040−3045.
(61) Huang, M.; Tian, J.; Zhou, C.; Bai, P.; Lu, J. Photoelectrochemical Determination for Acid Phosphatase Activity Based on an Electron Inhibition Strategy. *Sens. Actuators, B* **2020**, *307*, 127654.

https://doi.org/10.1021/acs.langmuir.1c01512
Langmuir XXXX, XXX, XXX−XXX